RSC Advances

ROYAL SOCIETY OF CHEMISTRY

www.rsc.org/advances

Coupled Electro-mechanic-chemical Dynamics Model for F_1F_0-motor

Lizhong Xu*, Yue Pan

* School of Mechanical Engineering, Yanshan University, Qinhuangdao 066004, China

Tel : + 86 335 8061472 , Fax :+ 86 335 8074783 , email : xlz@ysu.edu.cn

Abstract

F_1F_0-motor (ATP synthase) is a key link of the respiratory chain and its operation depends on the state and change of the respiratory chain. However, the relationship between these two has not yet been studied quantitatively. In this work, a coupled electro-mechanic-chemical dynamics model for F_1F_0-motor was established. The power system (respiratory chain) and the control system were considered together, and the coupled electro-mechanic-chemical equations were proposed. The dynamic response of the motor to the main control parameters and nerve pulse was studied. Some experimental observations were simulated and discussed. The model offered complete insight about the operation of F_1F_0-motor.

Keywords: F_1F_0-motor, respiratory chain, coupled model, control system, power system

Introduction

The blood pumping by the heart constitutes a form of mechanical work which is driven by cyclic contraction of cardiac myocytes. This energy for the contraction comes from the hydrolysis of ATP to ADP on mitochondrial membrane by F_1F_0-motor. Studying the operation mechanism of F_1F_0-motor is important for understanding the mechanism of the blood pumping by the heart and diagnosing heart diseases at the molecular level. F_1F_0-motor is driven by the proton gradient across the inner mitochondrial membrane (IMM) produced by Gibbs free energy from the redox span of the respiratory chain (see Fig.1a). The redox potential difference drives electrons to flow along IMM from complex I to IV where the electrons are gained by oxygen. Meanwhile, the redox potential is reduced and the potential energy is used to drive protons to pass through three proton pumps (complexes I, III and IV). This process results in the proton gradient across IMM consisting of an electrical and a chemical part. By the proton gradient, protons are driven to return to the inside of IMM through F_1F_0-motor that causes rotation of F_1F_0 and synthesis of ATP [1,2].

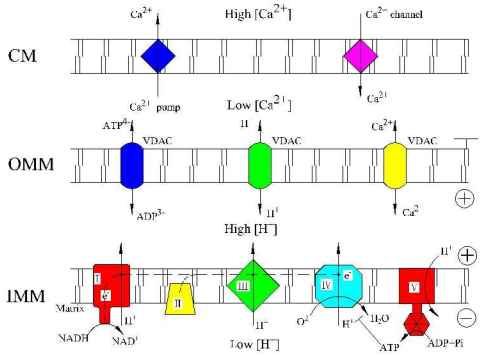

(a) General scheme of the oxidative phosphorylation system

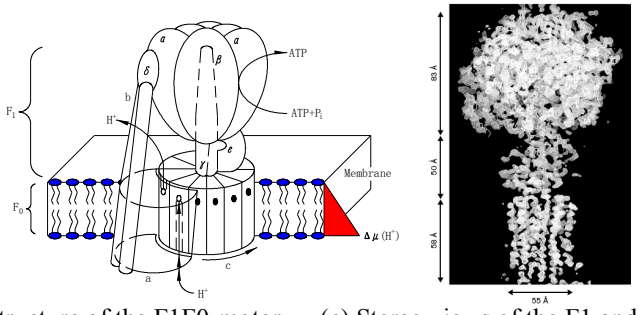

(b) Structure of the F1F0-motor (c) Stereo views of the F1 and c-ring complex

Fig.1 General scheme of the oxidative phosphorylation system and the structure of F1F0-motor. Reprinted with permission from AAAS [2].

To understand the operation mechanism of F_1F_0-motor, much research work has been done. A model for F_1F_0-motor was proposed which concluded that the F_1 motor achieved its high mechanical torque and almost 100% efficiency because it converted the free energy of ATP binding into elastic strain [3]. The structure of F_1 catalytic domain was studied and an electron density map of the F_1–c10 sub-complex was provided [4]. Based on the molecular mechanism, a kinetic scheme was developed and an expression was obtained to explain the pH dependence of the rate of ATP synthesis by ATP synthase [5]. The mechanisms of torque generation in the rotary F_0F_1-ATPase were discussed [6]. A detailed computer simulation of F_0 rotors was done to calculate and rationalize their selectivity, which concluded that H^+ selectivity was most likely a robust property of all F_0 rotors [7]. By molecular dynamics simulations of c-ring structures, a water channel as one of the half-channels was mapped and it was found that the channel was important to rotation in ATP synthesis mode [8]. A chemo-mechanical coupled model for rotation of the F_1F_0-motor was proposed, in which the movement of F_1, the movement of F_0, reactions at F_1 and reactions at F_0 were considered simultaneously [9]. A new structure of the c10 ring of the yeast mitochondrial ATP synthase was found, which represented the functionally open form of the c subunit to facilitate proton loading and release [10]. The possible necessity of the transmembrane helix TMH movements was investigated by assaying ATP driven H^+ pumping function before and after cross-linking paired Cys substitutions at the center of TMHs within subunit *a,* which suggested that the C-terminal domain of the cytoplasmic loop may function in gating H^+ translocation to the cytoplasm [11,12]. The state and change of the respiratory chain have important effects on the rotation rate and efficiency of the motor. The nerve pulse and calcium currents can cause sudden state change of the respiratory chain [13,14]. So far, the F_1F_0-motor has not been studied together with the respiratory chain and nerve pulse quantitatively yet.

Here, we propose a coupled electro-mechanic-chemical model for the F_1F_0-motor which includes the F_1F_0-motor, its power system (respiratory chain) and control system. The model is constructed in four steps. (1) A chemo-mechanic coupled model of the F_1F_0-motor is proposed. (2) An electro-chemical coupled model of the power system is proposed. An equivalent electric circuit for the power system is provided, and the proton gradient across IMM as a function of the redox potential difference, motor rotation rate and proton leak, etc. is studied. (3) An electro-chemical coupled model of the control system is proposed. Equations describing the dynamic response of the motor rotation rate to nerve pulse and other control parameters are presented. (4) Combining the three models above, a coupled electro-mechanic-chemical model is obtained. Using the model, several important problems are investigated: (1) Energy loss in the motor and its power system. (2) Change of the motor rotation rate along with the system parameters. (3) Dynamic response of the rotation rate to the control parameters and nerve pulse. (4) Dynamic response of the rotation rate and proton gradient in skeletal muscle and heart.

Methods

Chemo-mechanic coupled model of F_1F_0-motor:

The stochastic twisting wave of the elastic γ shaft can be described by its dynamic equation [9]

$$\tau_f + \tau_e + \tau_{fluct} + \tau_i = 0 \quad (1)$$

Here τ_f is the dynamic viscous torque on the γ shaft, τ_e is the elastic torsion torque in the γ shaft from its dynamic elastic deformation, τ_{flunct} is the Brownian torque from thermal fluctuation, and τ_i is the inertia torque in the γ shaft. They are functions of time and position.

It is known that the Reynolds number of the motion of molecular motor is small, as it is an over-damped system. However, thermal excitation may cause resonance wave of the γ shaft. The resonance speed is much higher than the rotation speed. Based on the model, the Reynolds number of F_1F_0 resonance is estimated at about 0.5-2. Therefore, the inertia of F_1F_0 should not be neglected.

According to Eq. (1), the natural frequencies, wave modes and stochastic response of the γ shaft to thermal excitation can be determined. The low frequency mechanical vibration modes of the γ shaft have larger vibration amplitudes than the high order modes. The large amplitude vibrations cause the escape of the gamma shaft from potential well easier. So, the wave amplitude and natural frequency of the lowest order mode plays an important role to the escape rate of the γ shaft from potential wells. The larger is the root-mean-square error of the wave amplitude, the larger the escape rate.

Another factor affecting the escape rate is the shift amount of the γ subunit and c-ring in potential wells. It can be obtained from the static torque balance equations of the γ shaft

$$\tau_{drive} - \tau_{load} - \tau_{eT} - \tau_{eP2} = 0 \quad \text{(c-ring in Arg 210 potential well)} \quad (2a)$$

$$\tau_{eT} - \tau_{eP1} = 0 \quad \text{(γ subunit in } F_1 \text{ potential well)} \quad (2b)$$

$$\tau_{drive} - \tau_{load} - \tau_{eT} - \tau_{f1} = 0 \quad \text{(outside of potential well)} \quad (2c)$$

Here τ_{drive} is the driving torque (proton gradient), τ_{load} is the load torque ($\tau_{load} = 3\Delta\mu_e/2\pi$, where $\Delta\mu_e$ is an amount of work hydrolyzing one ATP), τ_{eT} is the elastic torque from static twisting angle difference of the γ shaft at two ends, τ_{ePi} is the elastic torque from shift of the γ subunit or c-ring in potential wells ($\tau_{ePi} = -k_{Pi}\theta_{Pi}$, where θ_{Pi} is the shift amount, subscript i=1 for γ subunit and i=2 for c-ring), and τ_{f1} is the viscous torque on the actin filament or bead attached to γ protrusion or c-ring.

With the shift amount and root-mean-square error of the wave amplitude for the γ subunit and c-ring, the probability of the γ subunit or c-ring escaping from the potential wells can be calculated. Further, the oscillation time of the γ subunit or c-ring in each potential well can be given. Using Eq. (2c), the jumping time of c-ring from one potential well to another can be determined. Thus, the total time for 120^0 mechanical step is obtained.

Electro-chemical coupled model of the power system:

Electrons flow along a special path in IMM (see Fig. 2a). From complex I to complex IV, electrons shuttle between inner and outer sides. From inner side to outer side, the path of electron flow is coupled with the path of proton flow through proton pumps [15]. The redox potential energy is used to drive protons to pass through IMM. From outer side to inner side, the electron path is independent from the proton path. That can not cause proton flow in reverse. Here, we propose an equivalent circuit for the respiratory chain (see Fig. 2b):

The redox potential difference of the respiratory chain is applied to proton pumps in series. Thus, there is a transfer ratio which equals the shuttle time of electrons between inner and outer sides while flowing from complex I to IV. There is an outward rectification for protons in IMM and the membrane resistances can be considered as the diodes. With the proton gradient, the diode is in reverse cut-off state and the inward current (leak current) is quite small. With the electromotive force, the three proton pumps are conducted. Thus, a large proton flow passes through them and the proton gradient across IMM is maintained. Due to the proton gradient, the protons return to inner side of

IMM: one is the leak current; another is the current through F_1F_0-motor which drives the motor to rotate and synthesize ATP.

In Figure 2, ε is the redox potential difference of the respiratory chain, E is the electromotive force across proton pumps, r and I_e are the resistance and current of the electron circuit, respectively. V is the proton gradient across IMM, I_p is the leak current, I is the total proton current, I_H is the current through proton pumps, I_c is the current through membrane capacitance C_m, k is the transfer ratio ($k \approx \varepsilon / E$), and I_f is the current through the F_1F_0-motor ($I_f = \lambda f$, where f is the rotation rate of the motor, and λ is a coefficient). From Fig.2b, the electric circuit equations of the power system is given

$$\begin{cases} \varepsilon - rI_e = kE & \text{(3-a)} \\ E = V + R_H I_H & \text{(3-b)} \\ I = I_H + I_c & \text{(3-c)} \\ I_c = C_m\left(\dfrac{dE}{dt} - \dfrac{dV}{dt}\right) & \text{(3-d)} \\ V = V_s + \beta\int_0^t (I - \lambda f - I_p)dt & \text{(3-e)} \end{cases}$$

where V_s is static proton gradient, R_H conduction resistance of proton pumps, t the time, β is a constant.

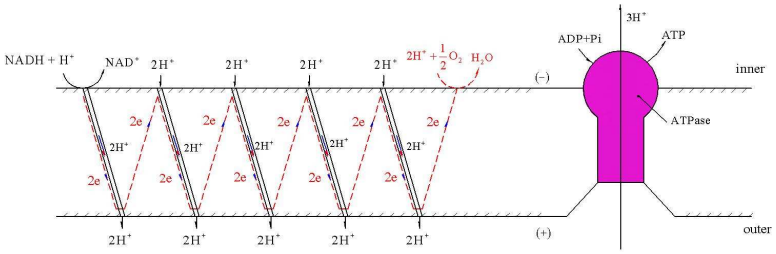

(a) Simplified model for the F1F0-motor and its driving system

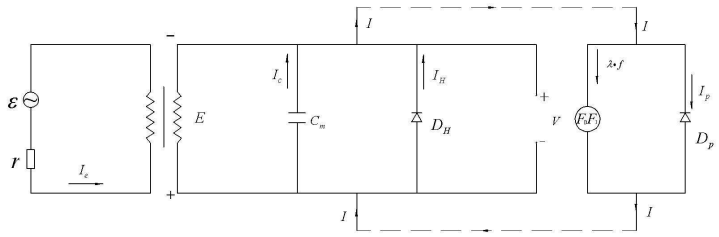

(b) Equivalent electric circuit for F1F0-motor and its power system

Fig.2 F1F0-motor and its driving system

For equilibrium state($I_c = 0$), Eq.(3-e) can be changed into $V = V_s$ and $I = \lambda f + I_p$. Substituting them into Eq.(3-a) and Eq.(3-b), the circuit equations of the power system in equilibrium can be given. From the final kinetic equation of the oxidative phosphorylation system, the electromotive force across proton pumps can be obtained. Combining it with Eq.(3), the coupled electrochemical equations of the power system are given.

It is known that the efficiency of the oxidative phosphorylation system is about 40%. So, the energy loss in its power system should be considered besides the mechanical energy losses in F_1F_0-motor. Among the power system, there are three places where loss of redox energy occurs(see Fig.2b). The first energy loss comes from the resistance to electron flow in the electron circuit(represented by electron circuit efficiency η_e).The second comes from the resistance to proton

flow in proton pumps(represented by proton pump efficiency η_p).The third comes from proton leak(represented by proton leak efficiency η_L).The efficiency(η) of the power system is given by $\eta = \eta_e \eta_p \eta_L$. Thus, the total efficiency of the motor and its power system is the efficiency(η) multiplied by mechanical efficiency of F_1F_0-motor.

Electrochemical coupled model of the control system:

Based on Eq. (3), the dynamic responses of the rotation rate f to the system parameters are

$$f(s) = E(s)\frac{G_1(s)G_2(s)}{1+\lambda G_2(s)} + D(s)\frac{g_D}{1+\lambda G_2(s)} + P(s)\frac{g_P}{1+\lambda G_2(s)} + \cdots \quad (4)$$

where $G_1(s) = \frac{1}{R_H} + C_m s$, $G_2(s) = g_v / G(s)$, $G(s) = \frac{1}{R_H} + C_m s + \frac{1}{\beta} s$, $g_v = \partial f / \partial V$, $g_D = \partial f / \partial [D]$, $g_P = \partial f / \partial [P]$.

From Eq. (4), the block diagram of the rotation rate control system for the F_1F_0-motor can be given as the black lines shown in Fig. 3. Further, the response of the rotation rate to changes of E , [D], and [P] etc. can be given. IMM is embraced by the outer mitochondrial membrane (OMM) where the voltage-dependent anion channel (VDAC) exists (see Fig. 1a). It is more permeable to anions than cations in the open state, which usually occurs with the membrane potentials lower than 10-20mV [16]. When the membrane potential is higher than 20 mV, VDAC undergoes transitions to multiple closed states and becomes more selectively permeable to cations [17]. In the open state, the fluctuating signals of the proton gradient across IMM can transfer to cell membrane (CM) through VDAC. In CM and ER membrane, calcium channels exist. The Ca^{2+} concentration is high outside of cell and inside ER. Usually, the calcium channel is close. When there are action potentials, CM is depolarized and the calcium channel is opened so that plenty of calcium ions flow into the cell and the mitochondria. Then, they are driven to return to the outside of cell (or inside of ER) by calcium pumps [18].

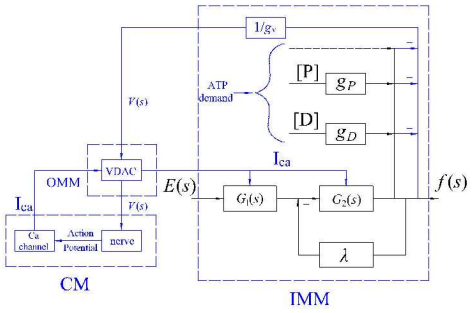

Fig. 3 The rotation rate control system for the F1F0-motor

As the electrochemical potentials change slowly, it can be approximately considered as equilibrium process. If they change suddenly, accelerating diffusion of ions will occur. Let $\left[Ca^{+2}\right]_{in}$ denote Ca^{2+} concentration inside a cell. Its diffusion acceleration can be expressed as $d^2\left[Ca^{2+}\right]_{in}/dt^2$. The dynamic equilibrium equation for Ca^{2+} diffusion can be written as $\mu_{in} = \mu_{out} - nF\Delta\phi + K\frac{d^2\left[Ca^{2+}\right]_{in}}{dt^2}$. Here, μ_{in} and μ_{out} are chemical potentials of Ca^{2+} inside and outside of CM, respectively. $\Delta\phi$ is the voltage across CM, n is the valence number, K is the coefficient representing the potential required for unit Ca^{2+} accelerating diffusion, $Js^2/(mol^2)$.

The first derivative of [Ca2+] plays a role of damping to [Ca2+] diffusion. It should cause an amplitude decay signal. However, from experimental observation in skeletal muscle [21] and heart [22], we know that the dynamic responses of the proton gradient are constant amplitude oscillation.

It means that the damping coefficient of the [Ca2+] diffusion is quite small. So, we neglected the first derivative of [Ca2+].

The voltage $\Delta\phi$ consists of the static ($\Delta\phi_s$) and dynamic ($\Delta\phi_d$) components. The concentration $\left[Ca^{+2}\right]_{in}$ consists of the static ($\left[Ca^{+2}\right]_{ins}$) and dynamic ($\left[Ca^{+2}\right]_{ind}$) components. Thus, the dynamic equilibrium equation above can be transformed into two equations: (1) a static equilibrium equation for static concentration; (2) a dynamic equilibrium equation for dynamic one. The dynamic equation is

$$\Delta\phi_d = L\frac{dI_{Ca}}{dt} + R_{Ca}I_{Ca} + \frac{1}{C}\int I_{Ca}dt \tag{5}$$

where I_{Ca} is the calcium current (mA/cm^2), $\left[Ca^{2+}\right]_{ind} = \frac{1}{\alpha}\int_0^t I_{Ca}dt$, R_{Ca} is the conduction resistance of calcium channel, $C = \alpha\left[Ca^{2+}\right]_{ins}\frac{nF}{RT}$ and $L = \frac{K}{\alpha nF}$ are denoted to be the equivalent capacitance and inductance of the calcium channel circuit, respectively.

With a nerve pulse, a number of Ca^{2+} flow into the mitochondria and prevent dephosphorylation and inactivation of NADH dehydrogenase. The protons pass through the proton pumps easily at high Ca^{2+} concentration. It means that high Ca^{2+} concentration causes significant decrease of the resistance of the proton pumps. The resistance R_H can be expressed as $\frac{1}{R_H(t)} = \frac{1}{R_{H1}} + (\frac{1}{R_{H2}} - \frac{1}{R_{H1}})\ I_{Ca}(t)$, where R_{H1} is the resistance before action potential, and R_{H2} is the resistance during action potential. Equation (5) gives the calcium current response to action potential ($\Delta\phi_d$). It causes sudden decrease of R_H and change of the proton gradient (V). From Eq. (3), the changes can be described by $C_m\frac{dV(t)}{dt} + [V(t) - E]\frac{1}{R_H(t)} = -\lambda f(t)$. Combining it with Eq. (5), the response of the motor rotation rate to action potential can be given. The control mechanics of the rotation rate of F_1F_0 motor is summarized as below:

With constant ATP demand, consumption and supply of ATP alternate, the concentrations of ATP and ADP in the mitochondrial matrix fluctuate periodically, which causes the periodical fluctuation of proton gradient across IMM. As ATP demand grows, the average concentration and its wave peak of ADP in the matrix grow. The rise of the average concentration causes decrease of the proton gradient across IMM and the electrochemical gradient across OMM. As the proton gradient is reduced to certain value, the electrochemical gradient across OMM becomes so small that periodical fluctuation of the proton gradient can initiate opening of VDAC in OMM. At the open state, both anions and cations can pass through VDAC easily. So, the fluctuating signals of the proton gradient across IMM can transfer to CM through VDAC and the action potentials are initiated. The action potentials make the calcium channels in CM open. Plenty of calcium ions flow into cell and mitochondria. So, a significant decrease of the resistance of proton pumps in IMM occurs and the rotation rate of F_1F_0 motor increases obviously.

In a word, OMM controls IMM by calcium current, and IMM controls OMM by proton gradient. From the insight and considering Eqs. (3) and (4), the block diagram of the rotation rate control system for F_1F_0-motor can be generalized from the black lines to blue lines in Fig.3.

Results and discussion

Figure 4 gives the efficiency of the power system of the F_1F_0 motor. It shows:

(1) The efficiencyη_T of the power system depends on the electron circuit efficiency (η_e), proton pump efficiency (η_p) and proton leak efficiency (η_L). As the proton gradient grows,η_T first grows, gets to its maximum value rapidly, and then changes slowly (here, I_f gets close to the maximum and I_p remains small). After some proton gradient, it drops rapidly.

(2) As the resistance R_H drops, the maximum η_T grows with the efficiency η_p, but the range of the electromotive force E for high η_T drops. As [D] grows, the maximum η_T changes little because η_p drops but η_L grows. However, the range of E for high η_T grows. For the non-activated state (R_H=1Ω/cm^2), the maximum η_T is about 70% (the energy loss from proton leak is about 9.8%, the energy loss from proton pump is about 20%, and the energy loss from electron transport is about 0.2%). If the mechanical efficiency of F_1F_0 is 72%, the maximum efficiency of F_1F_0 and its power system is about 50% for the non-activated state. For the activated state (R_H=0.2Ω/cm^2), the maximum η_T is about 85% (the energy loss from proton leak is about 7%, the energy loss from proton pump is about 7.9%, and the energy loss from electron transport is about 0.1%). If the mechanical efficiency of F_1F_0 is 72%, the maximum efficiency of F_1F_0 and its power system is about 60% for the activated state.

(3) If the electromotive force E is larger than certain critical value, η_T for large R_H is larger than that for small R_H. Otherwise, η_T for large R_H is smaller than that for small R_H. The critical value is 210mv and 230 mv for [D]=10μM and 60μM, respectively. Usually E is in the range of 210-250mV. So, with a given E, R_H drops with the rise of [Ca^{2+}], which makes the proton gradient rise and the motor rotation rate grow, and η_T drop (large E and low [D]) or rise (small E and high [D]). The former is identical to some known reports [19], while the latter gives another possible situation.

(4) As the motor rotation rate grows, η_T grows rapidly and gets to a high value, and then it remains in certain rate range with little change. As the rotation rate reaches some saturated value, η_T drops rapidly. As the resistance R_H grows ([D]=60μM and E=220mv), η_T drops obviously, but the rate range for highη_T is not changed. As [D] grows, the maximumη_T changes little, but the rate range for highη_T drops obviously.

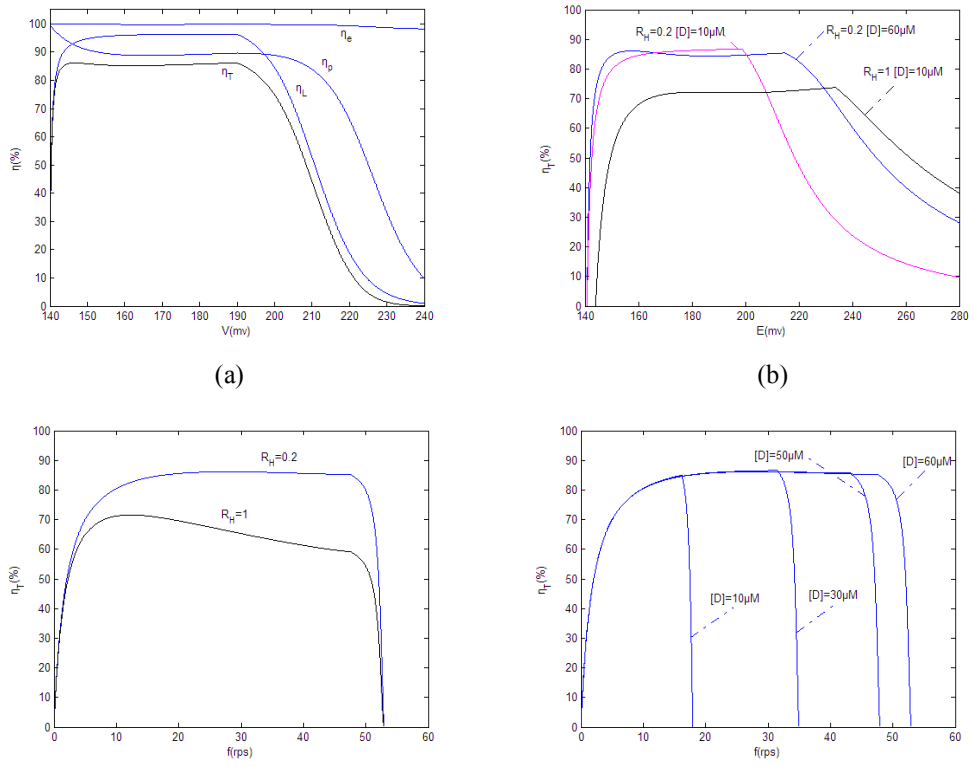

Fig.4 The efficiency of the power system

(a) changes of the efficiency with the proton gradient (b) changes of the efficiency with resistance RH, [D] and electromotive force E (c) changes of the efficiency with the rotation rate and resistance RH([D]=60μM and E=220mv) (d) changes of the efficiency with the rotation rate and [D](RH=0.2Ω/cm2)

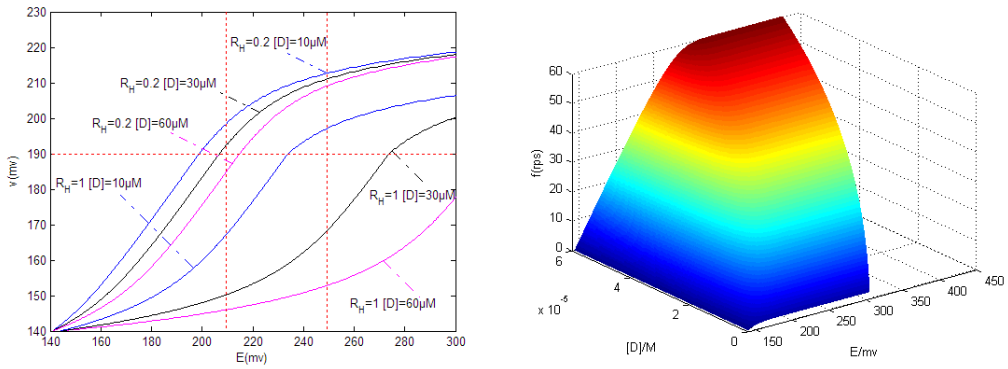

(a) changes of V along with E (b) f as a function of E and [D]

Fig. 5 Rotation rate f as a function of E, [D] and RH

It is known that there are three states in the mitochondria: over acidic state, over alkaline state and normal state. However, the difference of the rotation rate, system efficiency and redox potential under different states is not known yet. Figure 5 gives the rotation rate f as a function of E, [D] and R_H. Here E is taken as 140-300 mv, the load torque is 45 pNnm, [P]=1mM, [ATP]=10μM. The results together with the efficiency analysis above, give answers to the following questions:

(1) The proton gradient V is smaller than the electromotive force E due to the energy loss and resistance R_H. The energy loss depends on R_H and the proton current through proton pumps (it equals the leak current plus the current through F_1F_0). As E is lower than 220mv, V increases obviously with E. As E is higher than 220mv, V grows slowly because the leak current grows obviously.

(2) The protons can pass through proton pumps easily at high Ca^{2+} concentration (under nerve pulse), and the resistance R_H changes suddenly from a large value to a small one. So, the ATP turnover flux increases suddenly with constant E and [D]. It corresponds to the change from low work state to high work state. With a large R_H, the rotation rate grows slowly with E and [D]. It corresponds to the change from rest state to low work state.

(3) With constant E, the proton gradient V drops with increasing R_H or [D], because the energy loss on the resistance R_H grows. The larger is the resistance R_H, the more obvious effect of [D] on the proton gradient.

(4) With different E, there are three operating states in the mitochondria:

(i) When E=250-300mv, the proton gradient V is generally within the range of 190-250mv. It is proper for F_1F_0-motor as above stated, but the efficiency of its power system is low. So, it is not a proper range for the motor and its power system. Here, the efficiency is low and the rotation rate is large, the leak current and free radicals grow. Before and after action potential, the changes of the rotation rate are not evident. It corresponds to an over acidic mitochondria.

(ii) When E=140-210mv, the proton gradient V is within the range of 140-190mv. It is not proper for F_1F_0-motor, though the efficiency of its power system is high. So, it is also not a proper range for the motor and its power system. Here, the efficiency is high, but the rotation rate is small. Before and after action potential, the changes of the rotation rate are not obvious either. The production rate of ATP is smaller than its consumption rate, which will cause rapid increase of Ca^{2+} concentration and operation failure of the mitochondria. It corresponds to an over alkaline mitochondria.

(iii) When E=210-250mv, the proton gradient V is within the range of 140-190mv for the non-activated state (R_H=1Ω/cm^2), and within the range of 190-250mv for the activated state (R_H=0.2Ω/cm^2). Before and after action potential, the changes of the rotation rate are evident. It is the normal range for the motor and its power system.

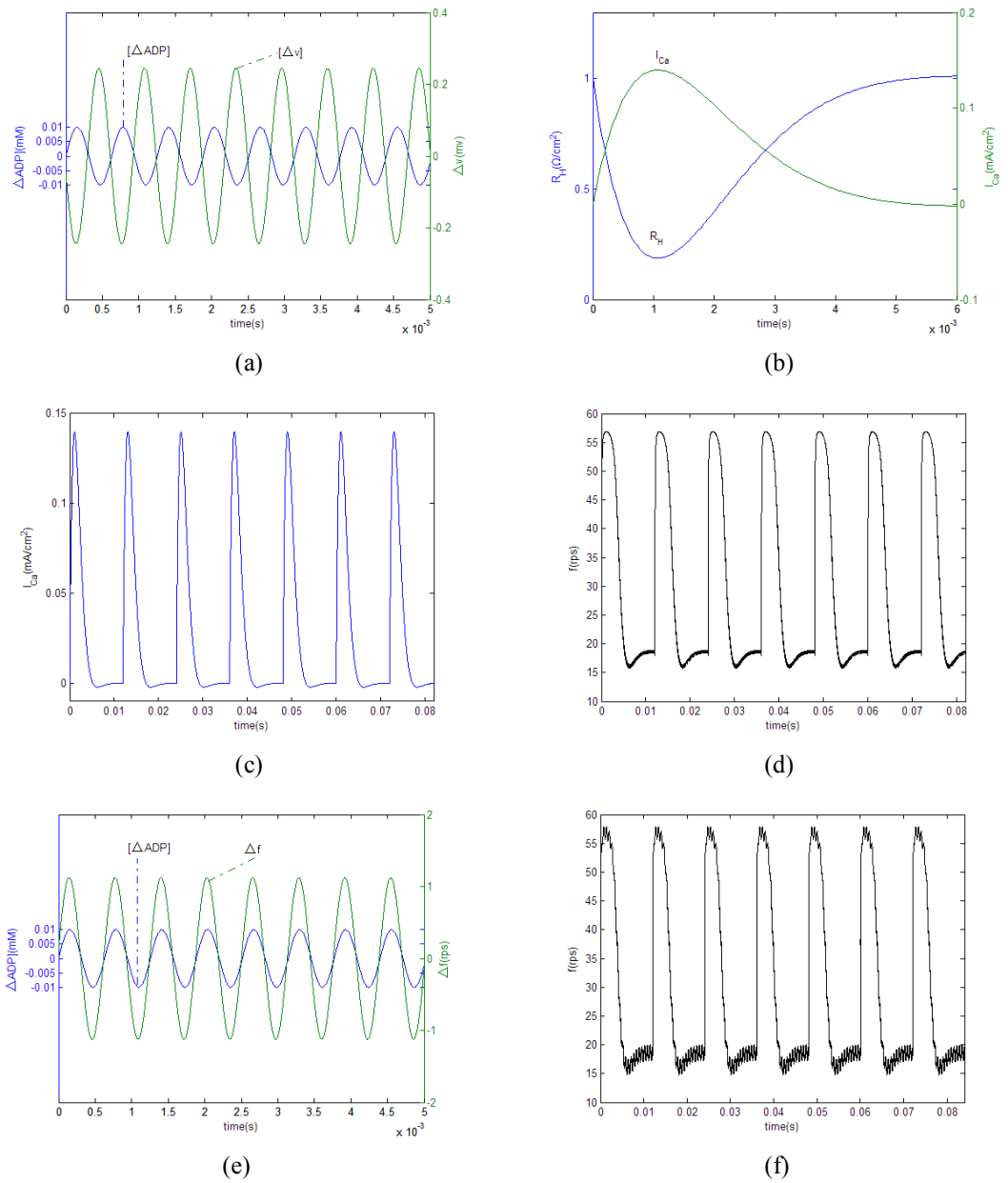

Fig.6 Dynamic response of the rotation rate to change of ATP demand

(a) fluctuation of [D] and proton gradient across IMM (b) pulse of calcium ions flow and RH drop (c) periodical pulse of calcium ions flow (d) periodical rises of the motor rotation rate (e) motor rotation rate fluctuation (f) total response of the rotation rate

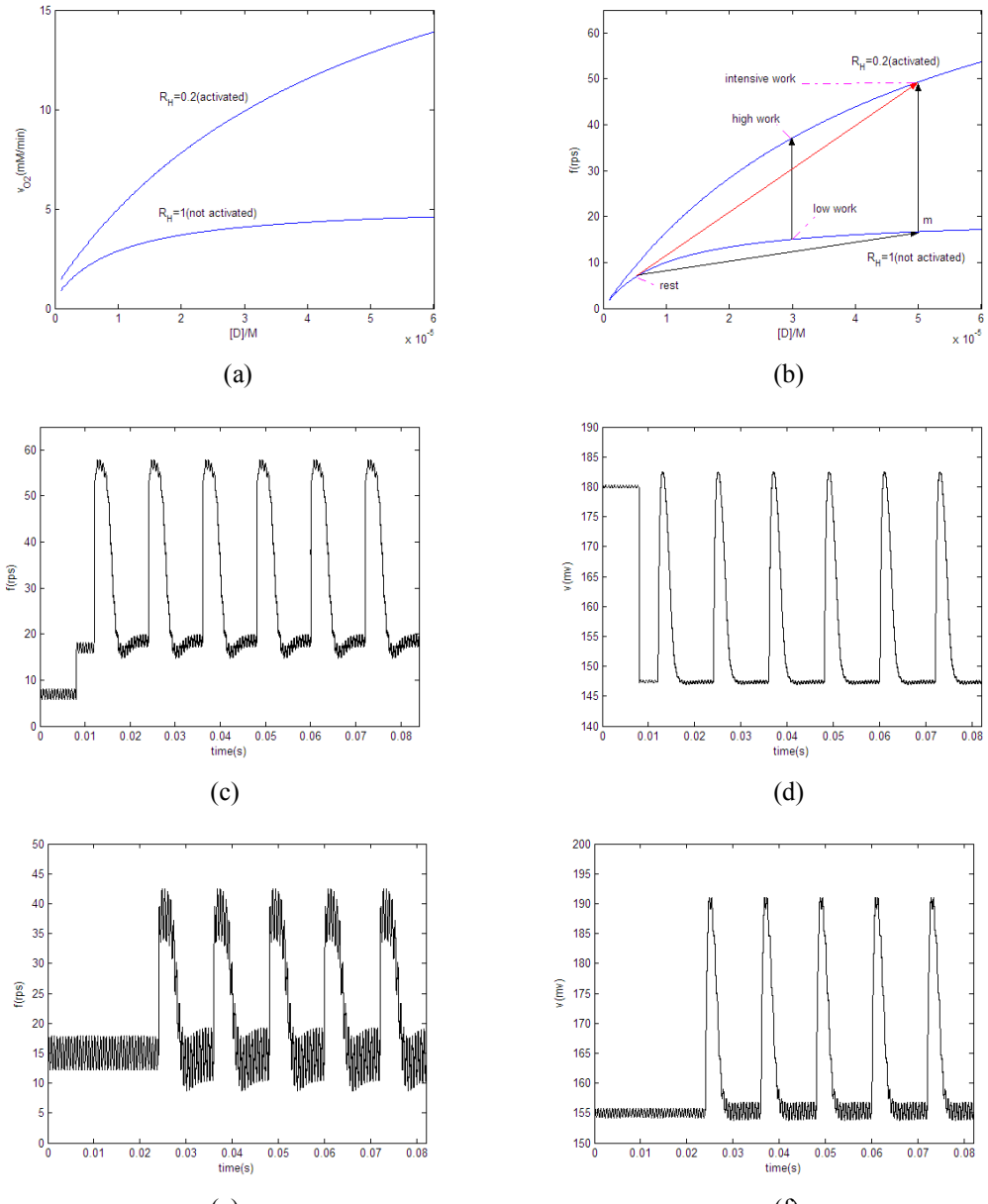

Fig.7 Dynamic responses of the rotation rate in skeletal muscle and heart
(a) change of VO2 along with [D] for different RH (b) change of f along with [D] for different RH (actually, Vo2 and f reach their minimal values at higher [D] in heart than in skeletal muscle, but it is ignored for simplifying purpose). (c) dynamic response of the rotation rate in heart (d) dynamic response of the proton motive force in heart (e) dynamic response of the rotation rate in muscle (f) dynamic response of the proton motive force in muscle

The main physiological extracellular regulatory stimuli that modulate the rate of ATP turnover are neural stimulation in skeletal muscle and heart. The secondary messengers that transfer the external signal to different processes involved in ATP consumption and production are Ca^{2+} ions. The neural stimulation is caused by the elevated energy demand, but the mechanism is not clear yet. It has not been studied how the neural stimulation initiates oxidative phosphorylation system. Here, the dynamic response of the rotation rate to the change of ATP demand (it corresponds to [D] changes) is investigated (see Fig. 6). The results together with the rotation rate control mechanics of the F_1F_0

motor above give novel explanation for the questions. It is shown that the key intermediate in oxidative phosphorylation system is the change and fluctuation of the proton gradient across IMM:
(1) If the ATP demand is constant, the average [D] also remains. However, the instant [D] fluctuates periodically, which can cause fluctuation of the proton gradient across IMM (see Fig.6a).
(2) As a nerve pulse is given, a pulse of calcium ions flow occurs that makes R_H drop rapidly (see Fig.6b). As multiple action potentials are given, a periodical pulse of calcium ions flow occurs that causes periodical rise of the motor rotation rate (see Fig.6c and d).
(3) The total response of the rotation rate is large periodical pulse plus small fluctuation (see Fig.6e and f). The average rotation rate of the motor decides ATP turnover rate. The larger is the frequency of the action potential, the larger the frequency of calcium ions pulse and ATP turnover rate. It was explained why the frequency of calcium pulses decides ATP turnover rate in literature [20].

There is an important difference between heart and skeletal muscle. In heart, the maximal relative increase of Vo_2 is moderate, and a perfect homeostasis of [D] is maintained during transition from low work to high work. As comparison, in skeletal muscle, the maximal relative increase of Vo_2 is much greater, and it is accompanied by a quite significant increase of [D] [21]. There remains debate about why the difference occurs between heart and skeletal muscle.

Hence, the changes and dynamic responses of the rotation rate in skeletal muscle and heart are studied(see Fig.7). The results offer quantitative explanation with a novel insight for the question above:
(1) Skeletal muscle
(i) For the skeletal muscle, the rest state exists ([D]<10μM) which corresponds to a respiration rate about 1mM/min (the rotation rate f of F_1F_0 is about 8rps). Given a nerve pulse, the intensive work state occurs and the respiration rate increases to 13mM/min (f is about 50rps). It involves state change of the system and rise of [D] (see Fig.7a and b).
(ii) The dynamic responses of the proton gradient V and rotation rate f to the nerve pulse are given in Fig.7c and d. At rest, f is low and V is high (about 180mv). As ATP demand grows, a rise of [D] occurs that makes f grow and V drop. When [D] rises to about 50μM, f gets to about 18rps, and V reduces to about 150mv. That makes the electrochemical gradient across OMM reduce to a critical value, so that periodical fluctuation of the proton gradient from [D] fluctuation can initiate opening of VDAC through which action potentials in CM are initiated.
(iii) The action potentials make calcium channels in CM open. Plenty of calcium ions flow into cell and mitochondria that prevents inactivation of NADH dehydrogenase. Thus, a significant decrease of the resistance of proton pumps in IMM occurs periodically, which causes periodical rises of V and f.
(iv) The peaks of the proton gradient V during action potential are close to that before action potential. V first changes from a high value to a low one, and then transits from a low value to a high one. After a peak, it comes back to the rest state and V returns to the initial high value. After that, the change and transition repeat periodically. The results are consistent with the experimental ones in reference [21]. That explains why the changes of proton gradient are small from rest to intensive work state in skeletal muscle [21].
(2) Heart

In heart, the rest state does not exist, and a low work state maintains ([D]≈30μM) which corresponds to a respiration rate about 3mM/min (f ≈15rps). Given nerve pulses, the high work state occurs and the respiration rate becomes about 10mM/min (f ≈40rps). It only involves the state change and does not involve the change of [D] (see Fig.7b).
(ii) The dynamic responses of the proton gradient V and rotation rate f to the nerve pulse are given in Fig.7e and f. At the low work state, f is low and V is also relatively low (about 155mv). As ATP demand grows, both the amplitude and frequency of [D] fluctuation become larger, which initiate opening of VDAC in OMM and the action potentials in CM. As the proton gradient is relatively low, a small increase of [D] fluctuation can just initiate VDAC, and it is not necessary that the average [D] grows and V drops. The results are consistent with the experimental ones in reference [22]. So,

before and after action potentials, the average [D] remains constant, which explains the experimental observation in heart [22].

Conclusions

In this paper, a coupled electro-mechanic-chemical model for F_1F_0-motor is proposed. The main work is summarized as below:

(1) It is known that there are three states in the mitochondria: over acidic state, over alkaline state and normal state. The difference of the rotation rate, system efficiency and redox potential under different states is explained.

(2) The main physiological extracellular regulatory stimuli that modulate the rate of ATP turnover are neural stimulation in skeletal muscle and heart. The secondary messengers that transfer the external signal to different processes involved in ATP consumption and production are Ca^{2+} ions. The neural stimulation is caused by the elevated energy demand, but the mechanism is not clear yet. It is not studied how the neural stimulation initiates oxidative phosphorylation system. The paper gives novel explanation for the questions. It is shown that the key intermediate in oxidative phosphorylation system is the change and fluctuation of the proton gradient across IMM.

(3) There is an important difference between heart and skeletal muscle. In heart, the maximal relative increase of Vo_2 is moderate, and a perfect homeostasis of [D] is maintained during transition from low work to high work. As comparison, in skeletal muscle, the maximal relative increase of Vo_2 is much greater, and it is accompanied by a quite significant increase of [D]. There remained debate about why the difference occurs between heart and skeletal muscle. The paper offers quantitative explanation for the question.

Acknowledgements

This material is based upon work supported by the Key Basic Research Foundation in Hebei Province of China (grant no. 13961701D)

References

[1] J.P. Abrahams, A.G.W. Leslie, R. Lutter, J.E. Walker, Structure at 2.8 A resolution of F–ATPase from bovine heart mitochondria, Nature 370 (6491) (1994) 621-628.

[2] D. Stock, A.G.W. Leslie, J.E. Walker, Molecular architecture of the rotary motor in ATP synthase, Science 286 (5445) (1999) 1700-1705.

[3] T. Elston, H.Wang, G. Oster, Energy transduction in ATP synthase, Nature 391 (6666) (1998) 510-513.

[4] S. Daniela, G. Clyde, A. Ignacio, G. Andrew, E.W. John, The rotary mechanism of ATP synthase, Current Opinion in Structural Biology 10 (6) (2000) 672-679.

[5] S. Jain, S. Nath, Kinetic model of ATP synthase: pH dependence of the rate of ATP synthesis, FEBS Letters 476 (3) (2000) 113-117.

[6] W. Junge, H. Sielaff, S. Engelbrecht, Torque generation and elastic power transmission in the rotary F0F1-ATPase, Nature 459 (7245) (2009) 364-370.

[7] A. Krah, D. Pogoryelov, J.D. Langer, P.J. Bond, T. Meier, J.D. Faraldo-Gómez, Structural and energetic basis for H(+) versus Na(+) binding selectivity in ATP synthase F(o) rotors, Bichimica et Biophysica Acta-Bioenergetics 1797 (6-7) (2010) 763-772.

[8] H. Gohlke, D. Schlieper, G. Groth, Resolving the negative potential (n-side) water accessible proton pathway of F-type ATP synthase by molecular dynamics simulations, Journal of Biological Chemistry 287 (43) (2012) 36536-36543.

[9] L. Xu, F. Liu, The chemo-mechanical coupled model for F1F0-motor, Progress in Biophysics and Molecular Biology 108 (3) (2012) 139-148.

[10] J. Symersky, V. Pagadala, D. Osowski, A. Krah, T. Meier, J.D. Faraldo-Gomez, D.M. Mueller, Structure of the c(10) ring of the yeast mitochondrial ATP synthase in the open conformation, Nature Structural & Molecular Biology 19 (5) (2012) 485-492.

[11] K.J. Moore, R.H. Fillingame, Obstruction of transmembrane helical movements in subunit a blocks proton pumping by F1Fo ATP synthase, Journal of Biological Chemistry 288 (35) (2013) 25535-25541.

[12] P.R. Steed, R.H. Fillingame, Residues in the polar loop of subunit c in Escherichia coli ATP synthase function in gating proton transport to the cytoplasm, Journal of Biological Chemistry 289 (4) (2014) 2127-2138.

[13] K. Bernhard, Intrinsic and extrinsic uncoupling of oxidative phosphorylation, Biochimica et Biophysica Acta 1604 (2) (2003) 77- 94.
[14] B. Kadenbach, S. Arnold, A second mechanism of respiratory control, FEBS Lett 447(2-3) (1999) 131-134.
[15] J. Koryta. Ions, electrodes and membranes, John Wiley & Sons, Journal of Electroanalytical Chemistry and Interfacial Electrochemistry 141 (5) (1982) 625-626.
[16] P. Evgeny, M.Sergey, L.M. Grigoriev, L. Chaninah, C.A.Zweihorn, K. Mannella, W. Kinnally, The mitochondrial channel VDAC has a cation-selective open state, Biochimica et Biophysica Acta-Bioenergetics 1710 (2-3) (2005) 96-102.
[17] K. Bernhard, Intrinsic and extrinsic uncoupling of oxidative phosphorylation, Biochimica et Biophysica Acta-Bioenergetics 1604 (2) (2003) 77-94.
[18] K.Bernard, Regulation of oxidative phosphorylation through parallel activation, Biophysical Chemistry 129 (2-3) (2007) 93-110.
[19] G. Michael, Influence of DNA stiffness in protein-DNA recognition. Journal of Biotechnology, 117 (2) (2000) 137-145.
[20] K.Bernard, Regulation of ATP supply in mammalian skeletal muscle during resting state→intensive work transition, Biophysical Chemistry 83 (1) (2000) 19-34.
[21] D.F.S.Rolfe, J.M.B. Newman, J.A. Buckingham, M.G. Clark, M.D. Brand, Contribution of mitochondrial proton leak to respiration rate in working skeletal muscle and liver to SMR, The American Journal of Physiology 276 (3 Pt 1) (1999) C692-C699.
[22] R.S. Balaban, H.L. Kantor, L.A. Katz, R.W. Briggs, Relation between work and phosphate metabolite in the in vivo paced mammalian heart, Science 232 (4754) (1986) 1121-1123.